Optimal Power Flow for Hybrid Ultracapacitor Systems in Light Electric Vehicles

Omar Laldin, Mazhar Moshirvaziri, Olivier Trescases
The Edward S. Rogers Sr. Electrical and Computer Engineering Department, University of Toronto
10 King's College Road, Toronto, ON, M5S 3G4, Canada

***Abstract*— This work demonstrates a predictive power optimization algorithm to control the power mix in a hybrid energy storage system, consisting of an ultracapacitor module and a lithium-ion battery pack for light electric vehicle applications. The algorithm uses a state-based approach, organized as a probability-weighted Markov process to predict future load demands. Decisions on power sharing are made in real-time, based on the predictions and probabilities of state trajectories along with associated system losses. A real-time global optimizer is then used to control the appropriate power mix using dc-dc converters. The full hybrid storage system, along with the mechanical drivetrain is implemented and validated experimentally on a 350 W, 50 V system with a programmable drive-cycle having a strong regenerative component. It is shown that the HESS system runs more efficiently and captures the excess regenerative energy that is otherwise dissipated in the mechanical brakes due to the battery's limited charge current capability.**

I. Nomenclature

I_{bt}	Battery terminal current [A]
$I_{bt}^{'}$	Battery converter output current [A]
I_{bt}^{*}	Battery converter output current command [A]
I_{bti}	Battery internal current [A]
I_{btp}	Battery parallel leakage current [A]
I_{uc}	U-cap terminal current [A]
$I_{uc}^{'}$	U-cap converter output current [A]
I_{uc}^{*}	U-cap converter output current command [A]
I_{uci}	U-cap internal current [A]
I_{ucp}	U-cap parallel leakage current [A]
I_{load}	Load current [A]
R_{btp}	Battery parallel resistance [Ω]
R_{bts}	Battery equivalent series resistance [Ω]
R_{uci}	U-cap internal series resistance [Ω]
R_{ucp}	U-cap parallel resistance [Ω]
R_{ucs}	Ultra-capacitor equivalent series resistance [Ω]
V_{bus}	System bus voltage [V]
V_{bt}	Battery terminal voltage [V]
V_{bti}	Battery internal voltage [V]
V_{uc}	U-cap terminal voltage [V]
V_{uci}	U-cap internal voltage [V]

II. Introduction

Efficient, cost-effective energy storage is one of the key enabling technologies for high performance electric vehicles (EVs). Automotive-grade ultracapacitors (u-caps) have been developed as a complimentary energy storage technology to batteries. Commercially available u-caps have symmetric input and output power densities on the order of 12 kW/kg [1], which is at least one order of magnitude higher then lithium-ion (Li-Ion) based batteries [2]. U-caps offer improved cycling lifetime and do not suffer as severely from high depth of discharge (DOD) effects as Li-Ion batteries [3].

The high power-density and low equivalent series resistance (ESR) of modern u-caps allow their integration into smart, electronically controlled hybrid energy storage systems (HESS) for light electric vehicles (LEVs). Effectively combining the high power-density feature of u-caps and the high energy-density of Li-Ion batteries is a major challenge. In conventional LEVs the excess regenerative power (regen) that cannot be safely absorbed by the battery must be dissipated in the mechanical brakes. The u-cap/battery HESS solution maximizes the re-use of regen energy, while reducing the strain on the battery during rapid acceleration. The reduction in the battery's peak power requirements due to the HESS extends the battery lifetime and also allows the use of the Li-Ion technologies having the highest possible energy density. The HESS concept has been previously studied through system-level simulations [3]–[7] with reported driving-range improvements of up to 46 % [4].

Numerous architectures can be used to interface the u-cap and battery in the HESS, some of which are discussed in [8]–[10]. In [3], the battery is directly connected to the inverter, while the u-cap is connected to the bus through a bidirectional dc-dc converter. Alternatively, the u-cap can be connected directly to the bus while the battery is connected through a bi-directional converter [8]. In the most flexible architecture, both energy sources are interfaced using dc-dc converters as shown in Fig. 1. This offers precise control of the power flow and increased flexibility in the choosing the operating voltages of the energy sources and the inverter, while increasing the system cost.

Several isolated and non-isolated dc-dc converter topologies have been considered for HESS, including resonant, boost, Cuk, and SEPIC/Luo. A soft-switching isolated converter suitable for HESS has been studied in [11]. Non-isolated converters offer low cost and volume [12], especially for the low-power applications covered in this work. The synchronous boost converter used in this work is deemed one of the best choices amongst the hard switching converters due to its simplicity and low cost [13]. The main focus of this paper is a new real-time predictive power optimization (PPO) block, inspired by the power-systems approach, to control the power flow in the HESS of Fig. 1.

This paper is organized as follows. Section III outlines the electrical system operation. The predictive power optimizer is described in Section IV. The system models used by the prediction algorithm are covered in Section V and experimental results are reported in Section VI.

III. Electrical System

The electrical LEV system used in this work is shown in Fig. 1. The u-cap and battery modules are interfaced with the DC bus, V_{bus} using two digitally-controlled synchronous dc-dc converters. Both phases operate in average current mode control (ACMC). V_{bus} is regulated to V_{ref}/K_{sense} by a high-bandwidth linear controller G_{v2}. The battery current reference, I^*_{bt}, is set by the PPO based on the algorithm described in Section IV. The PPO operates with a much lower bandwidth than G_{v2}. Using this scheme, I_{uc} is automatically adjusted by G_{v2} to account for the changes in I_{bt} and I_{load}, such that $I_{load} = I^{'}_{uc} + I^{'}_{bt}$, where $I^{'}_{uc}$ and $I^{'}_{bt}$ refer to the boost converter output currents. The system allows efficient bi-directional power flow between the two energy tanks and the mechanical load.

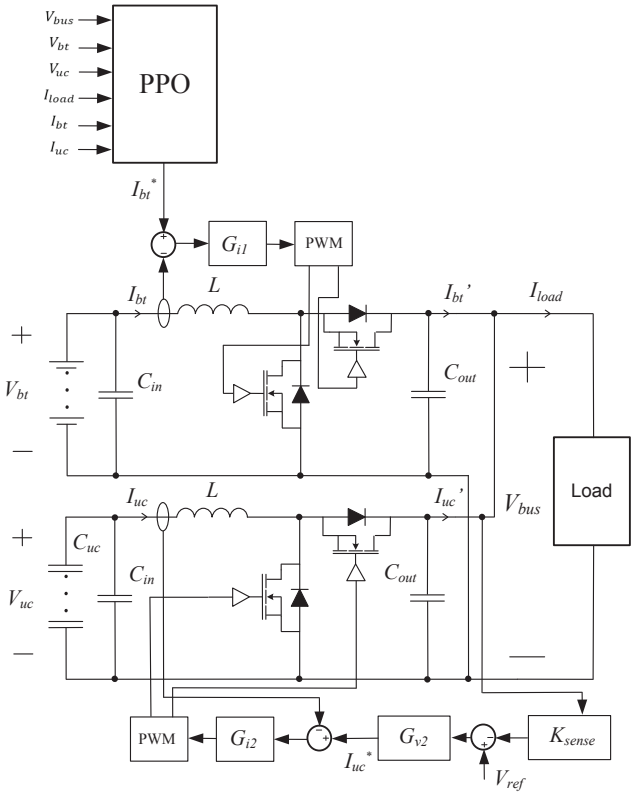

Fig. 1. Architecture for the hybrid u-cap/battery energy source.

IV. Predictive Power Optimizer

A. Overview

The PPO must estimate future power demands to optimize power flow in the HESS, since it does not have direct information about future drive-cycles. It must therefore optimize the dc-dc converter currents as the state and load current information becomes available. The algorithm determines the probability of future load currents and attempts to minimize losses within the prediction interval. A successful PPO must therefore (1) accurately predict the future power demands based on present information and statistical considerations and (2) make appropriate decisions regarding the power mix based on a search algorithm and loss models in the HESS elements.

When choosing an appropriate search algorithm to find the minimum cost (in terms of losses) power-mix, it is important to consider that the power transfer at each interface is constrained based on the maximum current limits and SOC of the storage devices. In order to allow the system to be scalable (with additional energy storage elements), it was decided to implement a non-gradient based, multivariate, constrained, search algorithm; the low-population strategy of the Differential evolution (DE) algorithm, with minimal cost evaluations.

B. Drive Cycle Data

An experimental drive-cycle for an electric bicycle is presented in [14]. By appropriately scaling the data, the expected drive-cycle of any LEV containing high variability in torque and speed can be roughly approximated. The scaled speed data is differentiated to obtain acceleration, which is then used to obtain the applied torque, based on a simplified mechanical model of an LEV. The torque and speed data are shown in Fig. 2 (a) and (b), respectively. The associated histogram of load currents is shown in Fig. 3. This distribution is used to design appropriate power converters in the HESS.

C. Operating States and Transitions

The representative drive-cycle is divided into time segments and represented by a statistical Markov process using a finite number of states, characterized by the speed and acceleration, with conditional probabilities assigned to the transitions. The process is shown in Fig. 4. The bus current is predicted at each state. Although a nine state process is shown, it was extended to a 5x5 transition matrix based on a reasonable trade-off between the prediction accuracy and the computational cost (determined through system simulations). The higher number of states allowed the speed and acceleration thresholds to be equidistant. The state matrix (and current predictions) are based on the reference drive-cycle. It is to be noted that the probabilities can be adjusted based on end-user behavior and regional terrain. With additional drive cycle data, the adaptive potential of the algorithm can be exploited for more accurate load prediction and loss minimization.

D. Cost Function and Constraints

A predictive cost function is developed based on the transition matrix of Fig. 4, whereby predicted load currents, along with a test vector (or power mix), are used to calculate system losses for three future time segments. Using the Markov process, a path matrix is first generated starting from the current state. The test power mix is used, along with the

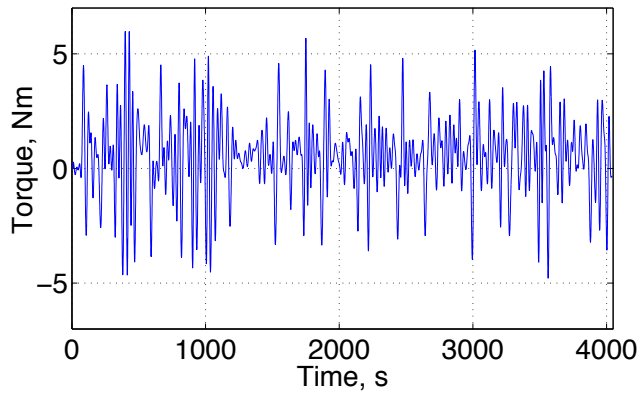

(a)

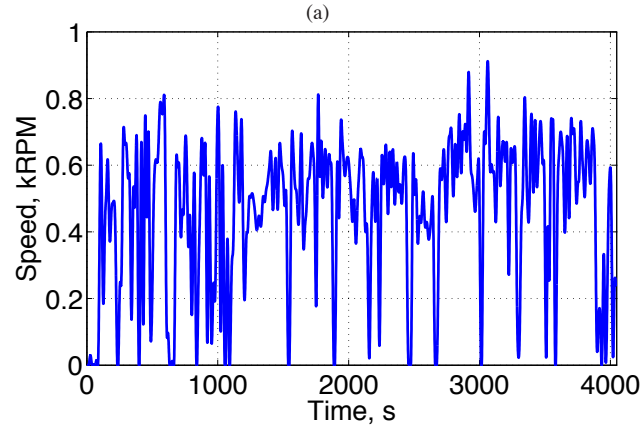

(b)

Fig. 2. Drive-cycle (a) torque and (b) motor speed data.

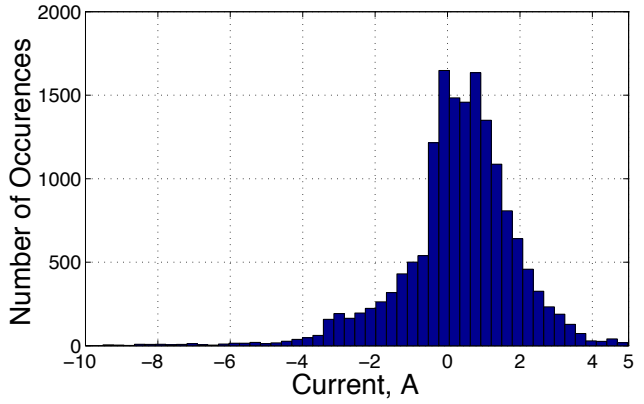

Fig. 3. Histogram of the load current for an LEV drive-cycle.

predicted I^*_{load} to determine I'_{uc} and I'_{bt}, and subsequently, I_{uc} and I_{bt} at the predicted states.

For each hypothetical future state, the state-of-charge (SOC) of the battery and u-cap is recalculated based on the inductor currents. The system losses at each state are calculated, summed for the path, and multiplied by the probability of going through that path. The loss calculations include the losses in the storage elements and the converter board. The losses in the inverter and drive train are ignored as they are

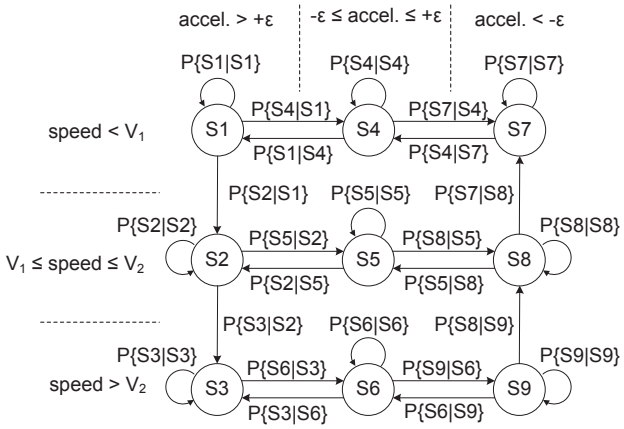

Fig. 4. The drive-cycle is represented as a Markov process with nine states. $P\{S_n|S_m\}$ represents the probability of entering state n from state m.

independent of the power mix. The cost function is the average of the probability-weighted costs. DE is used to provide a global optimum [15]. The battery SOC is tracked by coulomb-counting from the device terminals. A segment time of 5 s was used.

When V_{uc} is high, the energy transactions from the u-cap are cheaper than the high-ESR battery, in terms of energy loss. However, decreasing the u-cap SOC significantly increases the conversion ratio and losses for the boost converter (along with the transaction costs). The PPO may therefore completely avoid using the u-cap. To circumvent the issue, an adjustment function (1) was developed and multiplied to the u-cap phase losses.

$$f(SOC, I_{uc}) = 1 + sgn(I_{uc}) \cdot (1 - e^{-|I_{uc}|}) \cdot \left(\frac{SOC_{mid} - SOC}{SOC_{mid} - SOC_{min}} \right) \quad (1)$$

The multiplier above allows the PPO to accept transactions with marginally higher costs and artificially reduces the cost at low SOC, avoiding the trivial trajectory. Its effect is eliminated at the midpoint and maximized at the SOC endpoints. The multiplier can be considered as a correction factor for the inability of the algorithm to predict load currents farther than three states (or 15 s) ahead. A longer prediction would allow the algorithm to appreciate the benefits of maintaining charge on the u-cap for the overall drive cycle.

V. HESS Models

A. Li-ion Battery and Ultra-Capacitor Loss Models

The Li-ion battery is used as the primary energy storage element in the system. The battery has a limited energy efficiency and the voltage seen at the terminal of the battery, V_{bt}, is reduced by the battery ESR. The Li-ion battery chosen has a nominal voltage of 42 V and a storage capacity of 5.3 Ah. The charge and discharge currents are limited to 2 A and 12 A, respectively. The charge and discharge curves at 1, 3 and 5 A are shown in Fig. 5. The models for simulating these

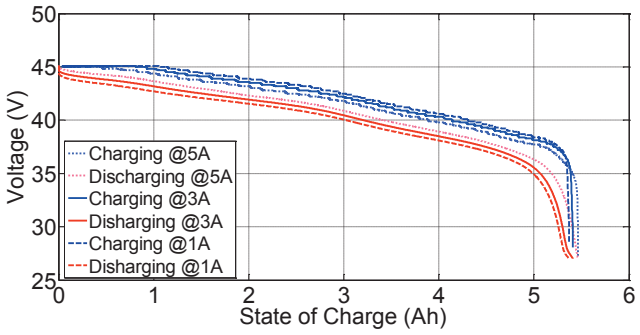

Fig. 5. Li-ion battery charge and discharge curves.

curves and are largely based on the internal cell voltage model proposed in [16].

$$V_{bti} = E_0 - K\left(\frac{Q_b}{Q_b - \int i \cdot dt}\right) + Ae^{-B\int i \cdot dt} \quad (2)$$

An external circuit is added to account for the limited coulometric efficiency in both the battery and the u-cap, as described below.

In the case of the u-cap, the internal source voltage, V_{uci}, is modeled by an ideal capacitor and is directly related to the accumulated charge and capacitance

$$V_{uci} = \frac{1}{C}\int i \cdot dt. \quad (3)$$

The energy storage devices are modeled by the circuit in

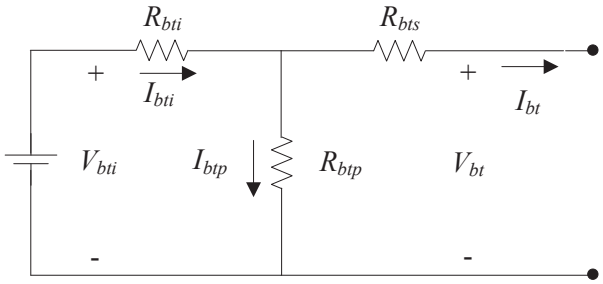

Fig. 6. Energy storage device model.

Fig. 6. The three resistors represent the power loss in the circuit for the given state voltages and currents. The u-cap model is identical, with different parameters.

To derive the power loss equations, it is assumed that I_{bt} behaves as a load in the positive direction and a source in the negative direction. Superposition is then used to determine the contributions of I_{bt} and V_{bti} to the total power loss. However, care must be taken to ensure that current dependencies across the parallel resistance (approximating both leakage and coloumetric loss) are accurately accounted for. During both charge and discharge, the contribution from both sources to I_{btp} is positive. Therefore, during discharge it is necessary to impose that the internal current I_{bti} is greater and is divided between I_{btp} and I_{bt}. During charge, I_{bt} is greater and is divided between I_{btp} and I_{bti}.

The charging case is considered first. The current contributions from I_{bt} and V_{bti} are added and result in the currents given as (4) and (5).

$$I_{bti} = \left(\frac{R_{btp}+R_{bts}}{R_{btp}}\right) I_{bt} + \left(\frac{V_{bti}}{R_{bti}+R_{btp}}\right) \quad (4)$$

$$I_{btp} = -\left(\frac{R_{bts}}{R_{btp}}\right) I_{bt} + \left(\frac{V_{bti}}{R_{bti}+R_{btp}}\right) \quad (5)$$

During discharge, the current contributions are given as (6) and (7).

$$I_{bti} = \left(\frac{R_{btp}}{R_{btp}+R_{bti}}\right) I_{bt} + \left(\frac{V_{bti}}{R_{bti}+R_{btp}}\right) \quad (6)$$

$$I_{btp} = -\left(\frac{R_{bti}}{R_{btp}+R_{bti}}\right) I_{bt} + \left(\frac{V_{bti}}{R_{bti}+R_{btp}}\right) \quad (7)$$

The power losses for the storage device are then obtained by summing the respective I^2R losses.

B. Converter Loss Model

Both dc-dc converters are modeled by the circuit shown in Fig. 7. The switch on-resistances are symmetric, $R_{1on} = R_{2on}$. Although the multi-phase converter is loaded by an electrical

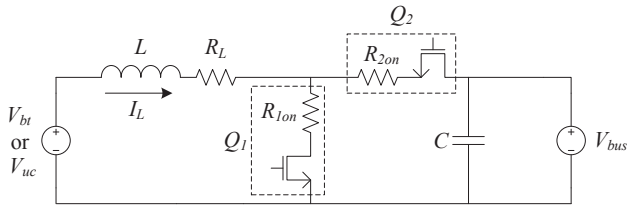

Fig. 7. Converter model.

motor-drive, it is sufficient to consider it as being loaded by an ideal current source $I_{bt}^{'}$ at a given time step. Using a time-averaged model, the duty cycle of the low-side switch for say, the battery phase can be determined as

$$D^{'} = \frac{V_{in} + \sqrt{V_{in}^2 - 4V_{bus}I_{out}(R_L + R_{on})}}{2V_{bus}}. \quad (8)$$

The input current is then $I_{in} = I_{out}/D^{'}$. The power loss in the converter includes the conduction I^2R loss and the switching losses. The switching losses are approximated as

$$P_{sw} = V_{bus} \cdot |I_{in}| \cdot f_{sw}(t_r + t_f). \quad (9)$$

VI. Experimental Results

The system of Fig. 8 was implemented using a flexible dynamometer experimental platform to evaluate the performance of the PPO under repeatable test conditions. The system parameters are provided in Table I. The dynamometer consists of

a permanent magnet synchronous machine (PMSM) loaded by a DC machine (DCM). The PMSM operates in torque-control mode, where τ_m is regulated using a three-phase inverter fed from V_{bus}. A two-quadrant chopper is used to control the speed ω_m in the DC machine. The electrical load on V_{bus}, P_{load} is therefore precisely emulated using the combination of the speed-controlled DCM and the torque-controlled PMSM, based on the drive-cycle of Fig. 2. The motor control is implemented in two real-time Linux (RTL) PCs. The PPO is implemented in real-time software and calculates I_{bt}^* every 500 ms.Two different tests were run: in Test #1 the u-cap is removed and the battery acts as the sole energy source. Test #2 was performed using the complete HESS system. In both tests, the ACMC dc-dc converter imposes a limitation on the maximum battery charge current, of I_{bt} >-2 A, This limitation is imposed to improve the long term state-of-health of the battery. In Test #1, large regen currents cause V_{bus} to increase when I_{bt} saturates to -2A. To emulate power otherwise dissipated in the mechanical brakes in the LEV, an electronic load is connected to the bus and programmed to absorb regen energy if V_{bus} >51 V.

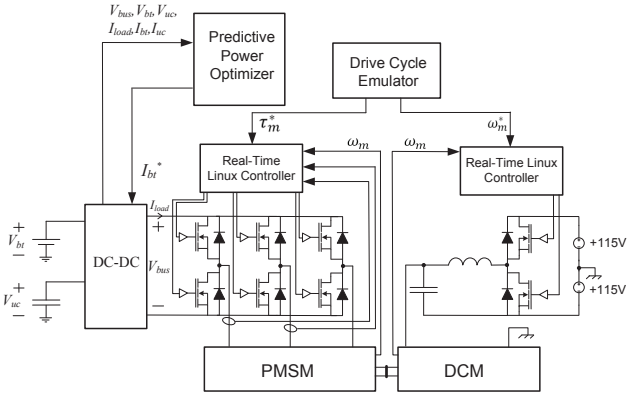

Fig. 8. Experimental system used to evaluate the PPO algorithm.

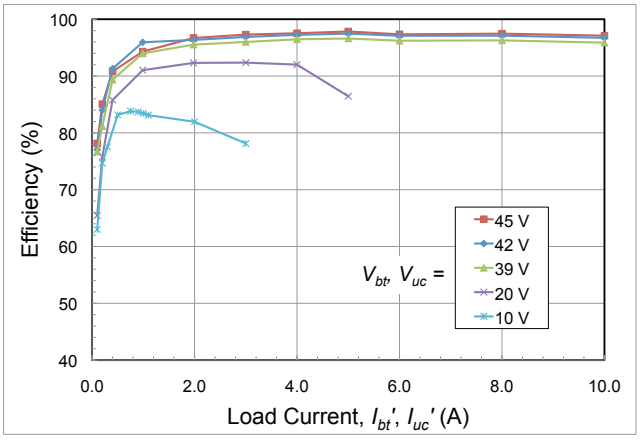

Fig. 9. Measured efficiency for the dc-dc converters with V_{bus} = 50.4 V.

The measured efficiency for each of the two dc-dc converters in Fig. 1 is shown in Fig. 9. The efficiency reaches a peak of 97 % but is reduced for lower input voltages, mainly due to the increased inductor current ripple. This justifies the need to keep V_{uc} high during operation. The SOC of the battery and u-cap during the HESS test is shown in Fig. 10. It is evident that the PPO attempts to maintain a reasonably high SOC on the u-cap in an effort to maximize efficiency. Fig. 11 shows the input and output currents from the dual-input, single output converter for 4.3 % of the full two-hour drive-cycle. The calculated and reference currents generated by the PPO during operation are also shown. As previously stated, the u-cap current reference $I_{uc}*$ is not used explicitly by the dc-dc converters. However, when compared against the current required to regulate the bus voltage, the reference and tested u-cap currents serve to validate the system models.

TABLE I
EXPERIMENTAL AND SYSTEM PARAMETERS

System Parameters	Value	Units
Bus Voltage, V_{bus}	50	V
Max. Power, P_{max}	350	W
Max. Current, I_{max}	7	A
Max. Torque, τ_{max}	7	Nm
Max. Speed, n_{max}	1000	RPM
Ultracapacitor Module		
Rated Capacity, Q_{uc0}	0.269	Ah
Base Voltage, V_{uc0}	27	V
Capacitance, C_{uc}	35.88	F
ESR, $R_{uc,esr}$	48	mΩ
Max. Dis/charge Current, I_{ucm}	+/-30	A
Mass	0.63	kg
Battery		
Rated Capacity, Q_{bt0}	5.3	Ah
O. C. Voltage, V_{bt0}	43.3	V
Measured ESR, $R_{bt,esr}$	268	mΩ
Max. Discharge Current, I_{btmp}	12	A
Max. Charge Current, I_{btmn}	2	A
Mass	4	kg
DC-DC Converter		
Input Capacitors, C_{in}	220	μF
Bus Capacitor, C_{bus}	5.02	mF
Switching Frequency, f_s	250	kHz
Inductors, L	10	μH
Inductor ESR, R_L	2.7	mΩ
Switch on-resistance, R_{on}	5	mΩ

The measured results of the two tests are given in Table II. The measured drive-cycle energy from the electrical data is slightly different in the two tests due to inevitable inaccuracies in the motor controllers. Due to this effect, Test #2 has an increase of 5.7 Wh in net energy demand from the drive-cycle compared to Test #1. Despite the increased demand, the total energy drawn from the battery in Test #2 is actually reduced by 7.2 Wh, mainly due to energy that is captured by the u-cap instead of being dissipated as braking losses. The HESS system results in a savings of 13 Wh. The average power loss

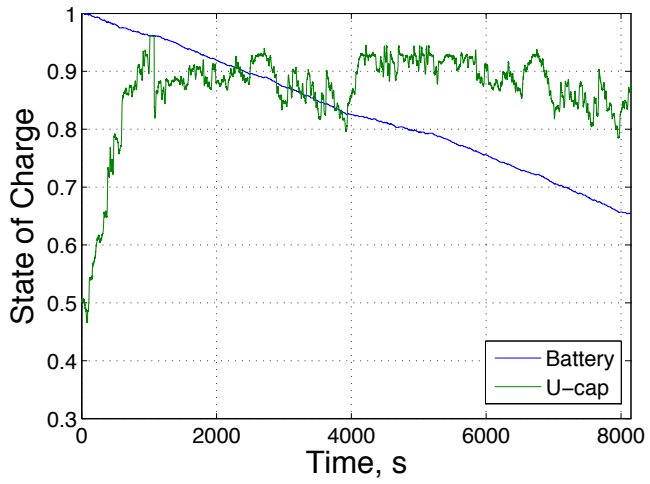

Fig. 10. Experimental battery and u-cap SOC.

was reduced from 10.5 W to 3.8 W from Test #1 to Test #2.

TABLE II
BATTERY AND HYBRID SYSTEM RESULTS

Energy Quantity	Test #1 Battery Only	Test #2 HESS	Units
Total Battery Energy Used	69.1	61.9	Wh
Drive-Cycle Energy (Sink)	98.0	103.3	Wh
Drive-Cycle Energy (Sourced)	-42.8	-42.4	Wh
Battery /and U-cap Loss	2.30	4.47	Wh
DC-DC Converter Loss	2.67	4.60	Wh
Braking Loss	18.7	2.3	Wh
Average Power Loss	10.5	3.8	W

VII. CONCLUSIONS

The predictive power optimizer was shown to successfully utilize the u-cap to buffer large negative currents on the DC bus that occur during regenerative braking. The power mix is controlled in real time based on the estimate of future power demand and a basic loss analysis. Future work will involve characterizing the PPO performance over a range of drive-cycles having various degrees of regenerative braking.

ACKNOWLEDGMENT

This work was supported by the Natural Sciences and Engineering Research Council of Canada, the Canadian Foundation for Innovation and the Ontario Research Fund. The authors wish to thank Prof. J. Tate from the University of Toronto for useful discussions related to power flow optimization.

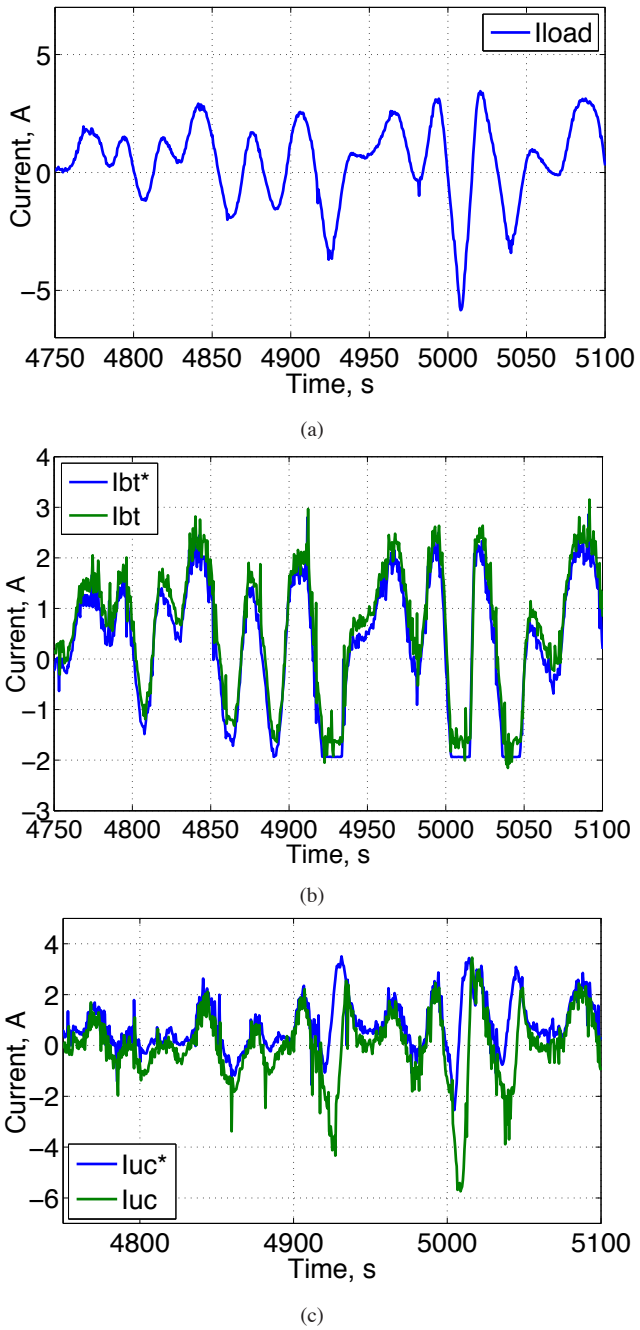

Fig. 11. Measured currents during the drive cycle for Test #2. a) Load current, I_{load} b) Battery current, I_{bt} c) U-cap current, I_{uc}.

REFERENCES

[1] "48 v ultracapacitor specifications," Maxwell Technologies Inc. Datasheet, 2010, available http://maxwell.interconnectnet.com/ ultracapacitors/datasheets/DATASHEET/48V/series/1009365.pdf.

[2] "U-charge xp lithium iron magnesium phospate battery," Valence Technology, datasheet, 2010, available http://www.valence.com/energy-storage/xp-12v-19v-lithium-phosphate-battery-module.

[3] A. H. A. Borhan, Vahidi, "Model predictive control of a power-split hybrid electric vehicle with combined battery and ultracapacitor energy storage," in *Proceedings of American Control Conference (ACC), 2010*, 2010, pp. 5031–5036.

[4] Z. B. W. C. J. Cao, B. Cao, "Energy-regenerative fuzzy sliding mode controller design for ultracapacitor-battery hybrid power of electric vehicle," in *Proceedings of IEEE International Conference on Mechatronics and Automation (ICMA), 2007*, 2007, pp. 1570–1575.

[5] T. U. K. Kawashima and Y. Hori, "Development of a novel ultracapacitor electric vehicle and methods to cope with voltage variation," in *Proceedings of IEEE Vehicle Power and Propulsion Conference (VPPC), 2009*, 2009, pp. 724–729.

[6] C. Z. X. Liu, Q. Zhang, "Development of a novel ultracapacitor electric

vehicle and methods to cope with voltage variation," in *Proceedings of IEEE Vehicle and Propulsion Conference (VPPC), 2009*, 2009, pp. 1395–1398.

[7] R. M. P. K. V. Shah, S. Karndhar and H. Desai, "An energy management system for a battery ultracapacitor hybrid electric vehicle," in *Proceedings of Int'l Conference on Industrial and Information Systems, 2009*, 2009, pp. 408–413.

[8] J. Cao and A. Emadi, "A new battery/ultra-capacitor hybrid energy storage system for electric, hybrid and plug-in hybrid electric vehicles," in *Vehicle Power and Propulsion Conference, 2009. VPPC '09. IEEE*, sept. 2009, pp. 941–946.

[9] S. Lukic, J. Cao, R. Bansal, F. Rodriguez, and A. Emadi, "Energy storage systems for automotive applications," *Industrial Electronics, IEEE Transactions on*, vol. 55, no. 6, pp. 2258 –2267, june 2008.

[10] S. Lukic, S. Wirasingha, F. Rodriguez, J. Cao, and A. Emadi, "Power management of an ultracapacitor/battery hybrid energy storage system in an hev," in *Vehicle Power and Propulsion Conference, 2006. VPPC '06. IEEE*, sept. 2006, pp. 1–6.

[11] K. Yamamoto, E. Hiraki, T. Tanaka, M. Nakaoka, and T. Mishima, "Bidirectional dc-dc converter with full-bridge / push-pull circuit for automobile electric power systems," in *Power Electronics Specialists Conference, 2006. PESC '06. 37th IEEE*, june 2006, pp. 1 –5.

[12] M. Dehaghi, R. Rajaei, and A. Ansari, "A new buck-and-boost ultra-capacitor interface circuit for the hevs," in *Industrial Electronics and Applications, 2009. ICIEA 2009. 4th IEEE Conference on*, may 2009, pp. 3382 –3387.

[13] R. Schupbach and J. Balda, "Comparing dc-dc converters for power management in hybrid electric vehicles," in *Electric Machines and Drives Conference, 2003. IEMDC'03. IEEE International*, vol. 3, june 2003, pp. 1369 – 1374 vol.3.

[14] S. O. O. Trescases and W. T. Ng, "Smart motor controller for an e-bike application," *IEEE Canadian Review*, no. 43, pp. 17–19, 2002.

[15] K. Price and R. Storn, "Differential evolution - a simple and efficient heuristic for global optimization over continuous spaces," *Journal of Global Optimization*, vol. 11, no. 4, pp. 341–359, 2002.

[16] L. D. O. Tremblay and A. Dekkiche, "A generic battery model for the dynamic simulation of hybrid electric vehicles," in *Proceedings of IEEE Vehicle Power and Propulsion Conference (VPPC), 2007*, 2007, pp. 284–289.